



# The effect of inlet temperature on the irreversibility characteristics of non-Newtonian hybrid nano-fluid flow inside a minichannel counter-current hairpin heat exchanger

Yulin Ma<sup>1,2</sup> · Majid Jafari<sup>3</sup> · Azeez A. Barzinjy<sup>4,5</sup> · B. Mahmoudi<sup>3</sup> · Samir M. Hamad<sup>6,7</sup> · Masoud Afrand<sup>8,9</sup>

Received: 3 April 2019 / Accepted: 6 August 2019  
© Akadémiai Kiadó, Budapest, Hungary 2019

## Abstract

The goal of this work is to examine the influence of entering temperature on the entropy generation characteristics of a minichannel hairpin heat exchanger with counter-flow configuration. The working fluids are water and hybrid water-Fe<sub>3</sub>O<sub>4</sub>/carbon nanotubes (CNTs) nano-fluid (NF) that flows through the annulus side and tube side of the heat exchanger, respectively. It is assumed that the NF is non-Newtonian, and its thermal conductivity and viscosity are temperature dependent. The impact of volume fraction of Fe<sub>3</sub>O<sub>4</sub> ( $\phi_{FF}$ ) and CNT nanoadditives ( $\phi_{CNT}$ ) as well as the Reynolds number of NF ( $Re_{nf}$ ) on the Bejan number and irreversibilities due to heat transfer and fluid friction are also assessed. It was found that augmenting the temperature difference between the fluids entering the heat exchanger results in a decrease in the frictional irreversibility and an increase in the global thermal and total irreversibilities and global Bejan number. Additionally, the outcomes depicted that the global frictional and total irreversibilities and the global Bejan number intensify by boosting the  $Re_{nf}$  and  $\phi_{CNT}$ , while the increase of  $\phi_{FF}$  first leads to the reduction and then the increase of these parameters.

**Keywords** Hybrid nano-fluid · Hairpin heat exchanger · Inlet temperature · Irreversibility · Carbon nanotube · Fe<sub>3</sub>O<sub>4</sub>

## List of symbols

$Be$  Bejan number  
 $c_p$  Specific heat (J kg<sup>-1</sup> K<sup>-1</sup>)

$d_{in}$  Inner diameter (m)  
 $d_{out}$  Outer diameter (m)  
 $k$  Thermal conductivity (W m<sup>-1</sup> K<sup>-1</sup>)  
 $p$  Pressure (Pa)

✉ Masoud Afrand  
masoud.afrand@tdtu.edu.vn

Yulin Ma  
ylma.hbwl@gmail.com

Azeez A. Barzinjy  
azeez.azeez@su.edu.krd

Samir M. Hamad  
samir.hamad@soran.edu.iq

<sup>1</sup> School of Electromechanical and Automobile Engineering, Huanggang Normal University, Huanggang 438000, P.R. China

<sup>2</sup> Suzhou Automotive Research Institute, Tsinghua University, Suzhou 215134, China

<sup>3</sup> Department of Mechanical Engineering, Kermanshah University of Technology, Kermanshah, Iran

<sup>4</sup> Physics Education Department, Tishk International University TIU, Erbil, Kurdistan Region, Iraq

<sup>5</sup> Physics Department, College of Education, Salahaddin University-Erbil, Kurdistan Region, Iraq

<sup>6</sup> Computer Department, Cihan University-Erbil, Erbil, Iraq

<sup>7</sup> Scientific Research Centre, Soran University, Soran, Kurdistan Region, Iraq

<sup>8</sup> Laboratory of Magnetism and Magnetic Materials, Advanced Institute of Materials Science, Ton Duc Thang University, Ho Chi Minh City, Vietnam

<sup>9</sup> Faculty of Applied Sciences, Ton Duc Thang University, Ho Chi Minh City, Vietnam

$Re$	Reynolds number
$\dot{S}_{g,f}'''$	Local frictional entropy generation rate ( $W m^{-3} K^{-1}$ )
$\dot{S}_{g,h}'''$	Local thermal entropy generation rate ( $W m^{-3} K^{-1}$ )
$\dot{S}_{g,t}'''$	Local total entropy generation rate ( $W m^{-3} K^{-1}$ )
$\dot{S}_{g,f}$	Global frictional entropy generation rate ( $W m^{-3} K^{-1}$ )
$\dot{S}_{g,h}$	Global thermal entropy generation rate ( $W m^{-3} K^{-1}$ )
$\dot{S}_{g,t}$	Global total entropy generation rate ( $W m^{-3} K^{-1}$ )
$T$	Temperature (K)
$u_{in,nf}$	Inlet velocity ( $m s^{-1}$ )
$V$	Velocity ( $m s^{-1}$ )

### Greek symbols

$\gamma$	Shear rate ( $s^{-1}$ )
$\mu$	Viscosity ( $kg m^{-1} s^{-1}$ )
$\rho$	Density ( $kg m^{-3}$ )

### Subscripts

nf	Nanofluid
w	Water

## Introduction

Today, many scientists and researchers around the world have become interested in nanotechnology as a field of science with extensive research domains. Truly, each branch of this science requires specialized and exclusive research, studies and experimentation. From the standpoint of advanced sciences, in industries related to medicine, energy, textile, vehicle manufacturing and many other applied science fields, nanotechnology has opened a new horizon to wonderful scientific innovations and provided suitable answers to many of human's scientific pursuits and enquiries.

One of the branches of nanotechnology relates to the use of nanoadditives with high thermal conductivity in base fluids with lower thermal conductivity. The product of this method is a suspension whose thermal properties is higher than that of the primary fluid used. This technique seems to be a suitable way to overcome the low efficiency problem associated with heat exchangers that use base fluids of low thermal properties as energy carriers. Choi [1] was the first researcher who succeeded in preparing these modern fluids, which he named "nano-fluids". Afterwards, extensive research works were conducted by various investigators throughout the world on the thermo-physical properties [2–10] and also the performance of these modern fluids in different equipment [11–19].

The NFs containing two or three solid nanoparticles are called hybrid NFs. In last year's, the hybrid nanofluids were utilized in different heat transfer applications as heat pipes, micro-channel, minichannel heat sink, solar systems, plate heat exchanger, air conditioning system, tubular heat exchanger, shell and tube heat exchanger, tube in tube heat exchanger and coiled heat exchanger, helical coil heat exchanger [20–30].

In recent years, the use of NFs to improve the efficiency of heat exchangers has attracted the attention of a group of researchers. The thermal conductivity of common heat transfer liquids is low and they can hardly meet the rising demand for cooling. Also, the conventional methods of improving the efficiency of heat exchangers, including the use of blades, turbulators, electric field and magnetic field, do not help much in this regard. Researches have shown that NFs can be a solution to this problem. In a numerical study, Goodarzi et al. [31] assessed the performance of a HPHE filled with nitrogen-doped graphene NF. It was found that the application of NF causes a 16.2% enhancement in the rate of heat transfer. Shahsavari et al. [32] carried out simulations to analyze the performance metrics of a HPHE filled with the aqueous CNT/Fe<sub>3</sub>O<sub>4</sub> hybrid NF from both first- and second-law perspectives. The outcomes revealed that boosting the  $Re$  and  $\phi$  causes an augmentation in the heat transfer. Karimi and Afrand [33] numerically assessed the influences of aqueous NF containing both the MgO and CNT nanoadditives on the performance of a heat exchanger. Both horizontal and vertical heat exchangers were evaluated in their work. They found that the horizontal heat exchanger performs better than the vertical one. Diglio et al. [34] studied the performance a borehole heat exchanger containing water–Ag, water–Cu, water–Al, water–Al<sub>2</sub>O<sub>3</sub>, water–CuO, water–Graphite, and water–SiO<sub>2</sub> NFs. The results showed the superior performance of the water–Cu NF as compared with the other NFs. Using the lattice-Boltzmann method, Rahimi et al. [35] analyzed the natural convection flow and heat transfer of water–CuO NF through a hollow heat exchanger considering nanoadditive shape effect. The results revealed the superior performance of NF with platelet type nanoadditives.

Literature survey demonstrates that the performance of NFs in heat exchangers has been studied mostly from the first-law viewpoint and that few research works have been carried out on the irreversibility aspects of heat exchangers filled with NFs. Using CFD simulation, Bahiraei et al. [36] examined the second-law performance of a counter-flow HPHE filled with water–CNT/Fe<sub>3</sub>O<sub>4</sub> hybrid NF. They reported that the entropy generation at low and high  $\phi$  is mainly due to the heat transfer and flow friction, respectively. Guzman et al. [37] used the CFD approach for assessing the entropy transportation process through a plate

and tube heat exchanger with elliptical and circular tubes and reported the better performance of the heat exchanger equipped with elliptical tubes. Dormohammadi et al. [38] executed the second-law analysis for flow of water–Cu NF through a wavy channel. The outcomes depicted that boosting the  $\varphi$  results in an enhancement in the thermal irreversibility. In addition, they found that the highest total irreversibility reduces by intensifying the Richardson number. Ebrahimi-Moghadam and Jabari Moghadam [39] utilized the irreversibility minimization approach to obtain optimal design characteristics of a corrugated channel filled with water–Al<sub>2</sub>O<sub>3</sub> NF. They reported that the application of NF with  $\varphi = 4\%$  causes 5% increase in the total irreversibility. Al-Rashed et al. [40] numerically investigated the impact of nanoadditive shape on the irreversibility aspect of boehmite alumina NF flow inside a HPHE. The results indicated that platelet and spherical type nanoadditives respectively represent the maximum and minimum irreversibilities.

To the best knowledge of the authors, the variation of irreversibility aspects of a HPHE in terms of entering temperatures of working fluids has not been assessed so far. The present numerical work is executed to fill this research gap. For this purpose, irreversibility characteristics of a HPHE containing water–CNT/Fe<sub>3</sub>O<sub>4</sub> NF are examined considering various entering temperatures. The influences of  $Re_{nf}$  as well as the  $\varphi_{CNT}$  and  $\varphi_{FF}$  on the thermal and fluid friction irreversibilities are also evaluated.

## Model configuration

### Geometry

Figure 1 depicts the schematic sketch of the studied HPHE. The length, inner diameter, and outer diameter of the heat exchanger are respectively 1 m, 1 mm, and 2 mm. The cold NF and hot water flow flows through the tube side and annulus side in a counter-flow manner. As shown in Fig. 1, the problem is modeled two-dimensionally which is because of the axial symmetry. The governing equations

are derived using the assumption of laminar and steady flow for incompressible fluids.

### Governing equations

In order to perform the simulations, the governing equations including conservation of mass, momentum and energy must be solved. These equations for the flow of water and NF are as follows [32]:

Continuity equation:

$$\nabla \cdot (\rho \mathbf{V}) = 0 \tag{1}$$

Momentum equation:

$$\nabla \cdot (\rho \mathbf{V} \mathbf{V}) = -\nabla p + \nabla \cdot (\mu \nabla \mathbf{V}) \tag{2}$$

Energy equation:

$$\nabla \cdot (\rho \mathbf{V} c_p T) = \nabla \cdot (k \nabla T) \tag{3}$$

### Boundary conditions

The adiabatic condition is imposed on the outer wall. Uniform velocity and uniform temperature are assumed at both tube and annulus inlets. The pressure outlet is selected for both the outlets. In addition, the no slip condition is used for the walls.

### Thermophysical properties of NF

In this research, the evaluated NF is a water based NF containing hybrid Fe<sub>3</sub>O<sub>4</sub>/CNT nanoadditives. For in detail discussion of the synthesis process of the NF, please consult with Shahsavari et al. [21–23]. In brief, the NF is synthesized by sonicating the sufficient volume of aqueous Fe<sub>3</sub>O<sub>4</sub> and CNT NFs for 5 min. The size analysis revealed that the average diameter of the prepared hybrid nanoparticles is 59.3 nm. The  $\varphi_{FF}$  and  $\varphi_{CNT}$  of the examined NFs along with their specific heat and density are reported in Table 1.

The results of rheological test revealed that the water–CNT/Fe<sub>3</sub>O<sub>4</sub> NF present non-Newtonian pseudoplastic behavior such that the viscosity drops sharply with the

Fig. 1 Geometry of problem

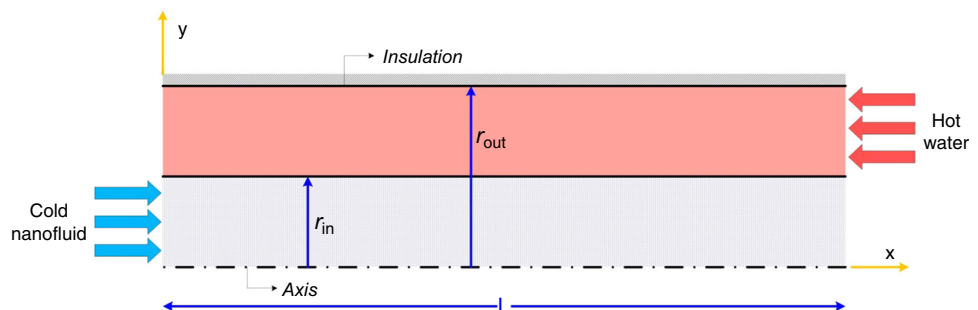


**Table 1** Characteristics of the studied nano-fluid samples [14]

Sample name	Fe <sub>3</sub> O <sub>4</sub> /vol%	CNT/vol%	ρ <sub>nf</sub> /kg m <sup>-3</sup>	C <sub>p,nf</sub> /J kg K
0.1%FF	0.1	0	1000.953	4160.557
0.5%FF	0.5	0	1016.765	4094.560
0.9%FF	0.9	0	1032.577	4028.563
0.9FF% + 0.45%CNT	0.9	0.45	1037.541	3997.691
0.9%FF + 0.9%CNT	0.9	0.9	1042.504	3967.114
0.9%FF + 1.35%CNT	0.	1.35	1047.468	3936.826

increasing shear rate. In addition, it was found that the viscosity reduces by boosting the temperature and intensifies by enhancing the φ<sub>FF</sub> and φ<sub>CNT</sub>. Moreover, experimental findings show that the thermal conductivity of the considered NF boosts with intensifying the temperature, φ<sub>FF</sub> and φ<sub>CNT</sub>. After performing the required tests, and using the artificial neural network, a relationship was established to forecast the thermal conductivity and viscosity versus temperature, φ<sub>FF</sub> and φ<sub>CNT</sub>, and shear rate (only for viscosity) [41]. Figure 2 shows that the developed models can predict the thermal conductivity and the

viscosity with high precision. It should be noted that the obtained models are valid within the temperature range of 25–55 °C, Fe<sub>3</sub>O<sub>4</sub> concentration range of 0–0.9%, CNT concentration range of 0–1.35%, and shear rate range of 1–100 s<sup>-1</sup>.

The Reynolds number of NF (*Re<sub>nf</sub>*) and water (*Re<sub>w</sub>*) can be computed through the following formulas:

$$Re_{nf} = \frac{\rho_{nf} u_{in,nf} d_{in}}{\mu_{nf}} \tag{4}$$

$$Re_w = \frac{\rho_w u_{in,w} (d_{out} - d_{in})}{\mu_w} \tag{5}$$

where *u<sub>in,nf</sub>* is the entering velocity of NF and *u<sub>in,w</sub>* is the entering velocity of water.

**Irreversibility analysis**

The irreversibility in the flow field has two main sources including the heat transfer and flow friction. The local frictional (*S<sub>g,f</sub><sup>'''</sup>*) and thermal (*S<sub>g,h</sub><sup>'''</sup>*) irreversibility as well as the total irreversibility (*S<sub>g,t</sub><sup>'''</sup>*) are calculated through the following formulas [42]:

$$\dot{S}_{g,f}''' = \frac{\mu_{nf}}{T} \left\{ 2 \left[ \left( \frac{\partial v_x}{\partial x} \right)^2 + \left( \frac{\partial v_y}{\partial y} \right)^2 \right] + \left( \frac{\partial v_x}{\partial y} + \frac{\partial v_y}{\partial x} \right)^2 \right\} \tag{6}$$

$$\dot{S}_{g,h}''' = \frac{k_{nf}}{T^2} \left[ \left( \frac{\partial T}{\partial x} \right)^2 + \left( \frac{\partial T}{\partial y} \right)^2 \right] \tag{7}$$

$$\dot{S}_{g,t}''' = \dot{S}_{g,f}''' + \dot{S}_{g,h}''' \tag{8}$$

The global irreversibilities are computed from the integration of the local irreversibilities over the whole domain as follows [42]:

$$\dot{S}_{g,f} = \int \dot{S}_{g,f}''' dV, \dot{S}_{g,h} = \int \dot{S}_{g,h}''' dV, \dot{S}_{g,t} = \int \dot{S}_{g,t}''' dV \tag{9}$$

The Bejan number is defined to determine the contribution of each factor in irreversibility generation. It indicates the ratio of thermal irreversibility to the total irreversibility as below [17]:

$$Be = \frac{\dot{S}_{g,h}}{\dot{S}_{g,t}} \tag{10}$$

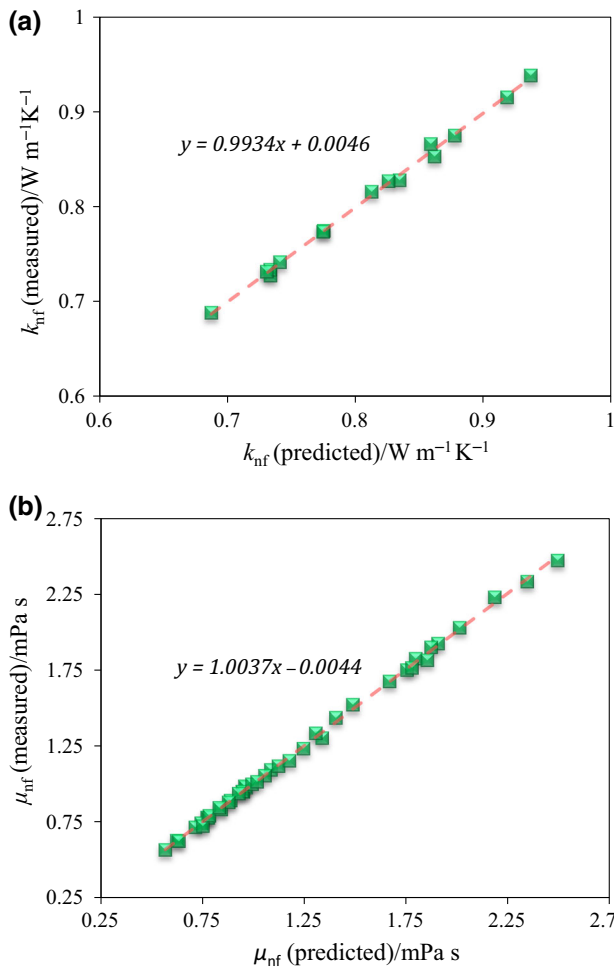


**Fig. 2** Comparison of outcomes by experiments and developed models for **a** thermal conductivity, **b** viscosity [41]

### Numerical method and validation

The control volume technique is employed to solve the governing Eqs. (1)–(3). The coupling between pressure and velocity is modeled by SIMPLE method. Second order upwind scheme is applied for discretizing the convective and diffusive terms in the governing equations. As convergence criteria,  $10^{-6}$  is chosen for all dependent parameter. A structured rectangular mesh is utilized to discretize the computational domain in this study. A grid refinement is used close to the walls to capture the high temperature and velocity variations. The grid independence examination was carried out by comparing the pressure loss and heat transfer rate of hybrid NF containing  $Fe_3O_4$  and CNT nanoadditives with volume concentration of 0.9% and 1.35%, respectively, at  $Re_{nf} = 2000$ ,  $Re_w = 1000$ ,  $T_{in,nf} = 298K$  and  $T_{in,w} = 308 K$  for different grid sizes. It is observed in Table 2 that the grid system of  $1000 \times 45 \times 45$  (in  $x$ ,  $y$  direction of tube side and  $y$  direction of annulus side, respectively) is chosen as the most appropriate grid.

In order to confirm the validation of the results, the data presented in this contribution is compared with the data provided in the experimental work of Duangthongsuk and Wongwises [43] for flow of water– $TiO_2$  NF in a HPHE. The outcomes are reported in Table 3 and it can be seen that there is an excellent match between the two results.

### Results and discussion

In this numerical investigation, the influences of entering temperatures of working fluids on the irreversibility metrics of a HPHE containing water–CNT/ $Fe_3O_4$  NF are examined. The numerical simulations are carried out at  $\phi_{FF}$

of 0 to 0.9%,  $\phi_{CNT}$  of 0–1.35%,  $Re_{nf}$  of 500–2000, NF entering temperature of 298 K, water entering temperature of 308–338 K, and  $Re_w = 1000$ .

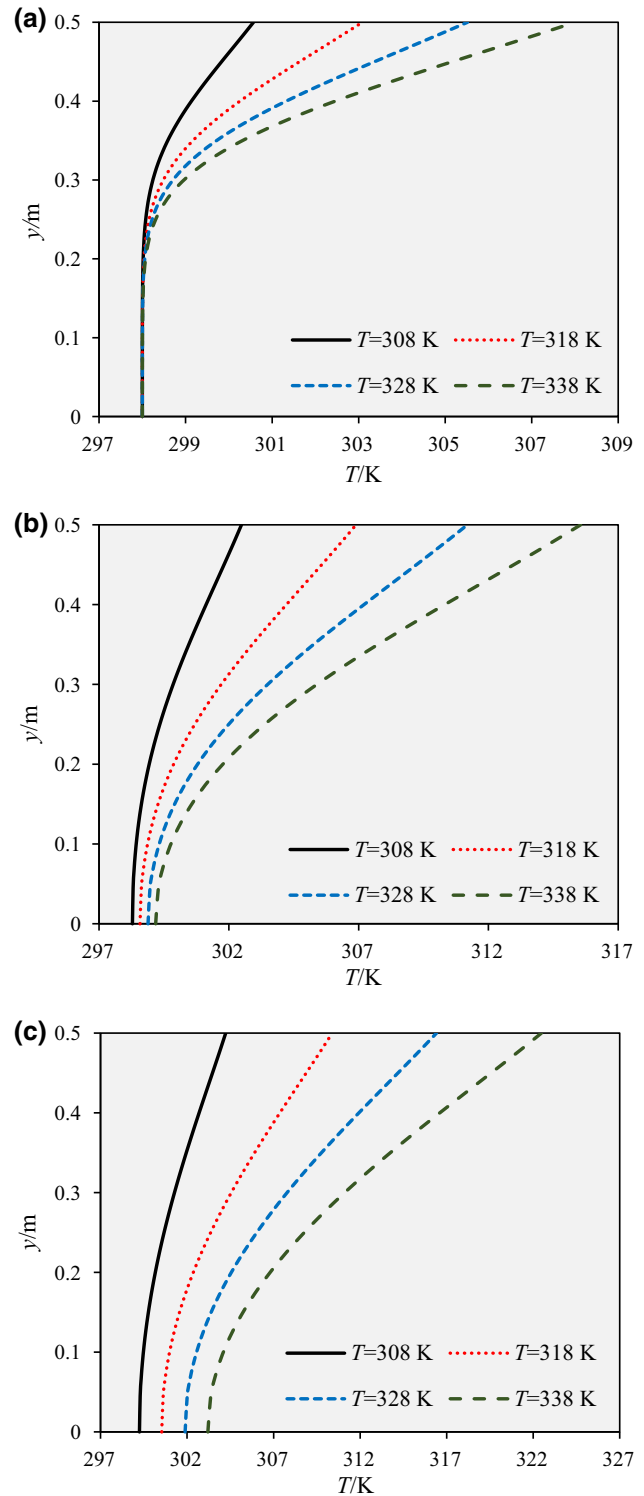


**Fig. 3** Temperature profile at cross section **a**  $x = 0.1m$ , **b**  $x = 0.5m$  and **c**  $x = 0.9m$  at various entering water temperatures for  $\phi_{FF} = 0.9\%$ ,  $\phi_{CNT} = 1.35\%$  and  $Re_{nf} = 2000$

**Table 2** Findings of grid independent test

Mesh	$\dot{Q}/W$	Error/%	$\Delta p/KPa$	Error/%
$800 \times 35 \times 35$	38.123		173.391	
$900 \times 35 \times 35$	42.289	10.93	184.333	6.31
$1000 \times 40 \times 40$	44.951	6.29	192.444	4.40
$1000 \times 45 \times 45$	46.728	3.95	196.37	2.04
$1200 \times 50 \times 50$	47.377	1.39	199.345	1.51

**Table 3** Comparison between results obtained from present study and experimental results [43]

$Re$	$Nu$ [43]	$Nu$ (present)	Error/%
8900	90.38	85.82	5.05
10,450	98.44	98.90	0.47
11,820	105.82	106.50	0.64
13,200	114.56	114.66	0.09
14,500	120.60	123.51	2.41

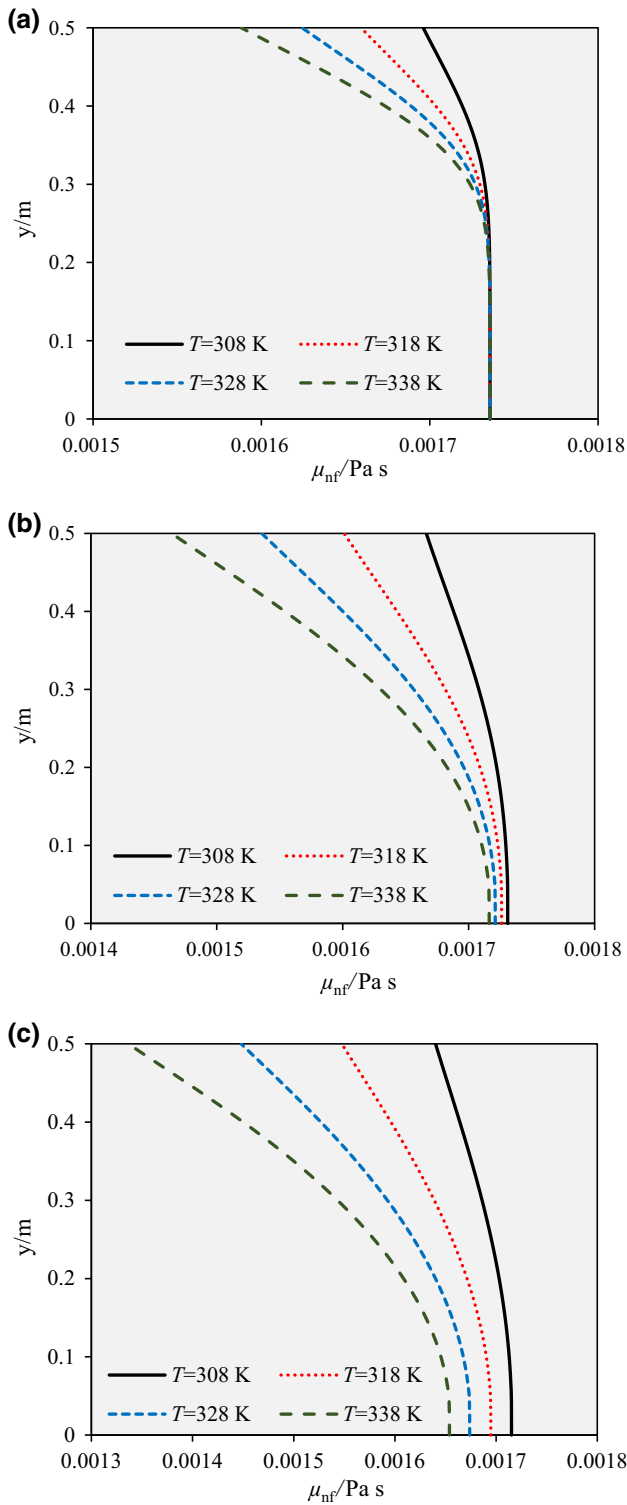


**Fig. 4** Viscosity profile at cross section **a**  $x = 0.1\text{m}$ , **b**  $x = 0.5\text{m}$  and **c**  $x = 0.9\text{m}$  at various entering water temperatures for  $\varphi_{\text{FF}} = 0.9\%$ ,  $\varphi_{\text{CNT}} = 1.35\%$  and  $Re_{\text{nf}} = 2000$

Figure 3 gives the temperature profile of NF versus entering water temperature along the cross sections  $x = 0.1, 0.3$  and  $0.9\text{m}$ . For all the considered cross

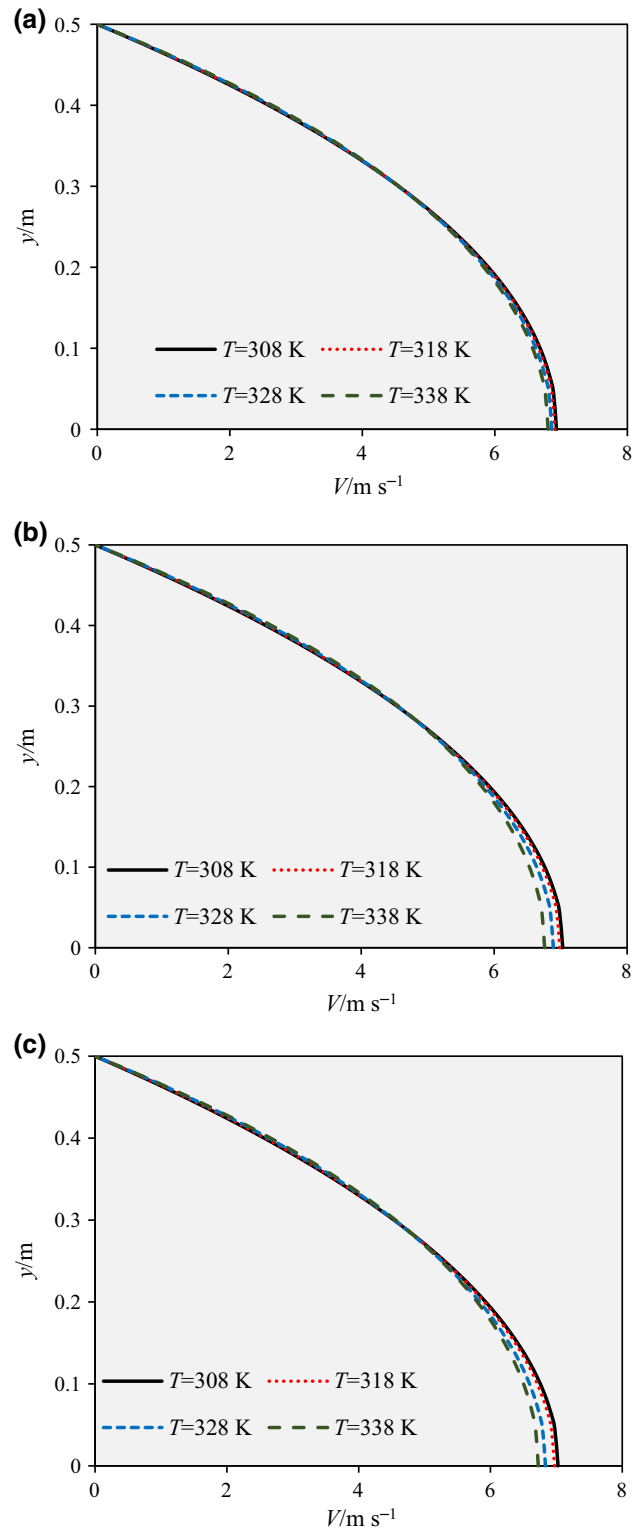


**Fig. 5** Velocity profile at cross section **a**  $x = 0.1\text{m}$ , **b**  $x = 0.5\text{m}$  and **c**  $x = 0.9\text{m}$  at various entering water temperatures for  $\varphi_{\text{FF}} = 0.9\%$ ,  $\varphi_{\text{CNT}} = 1.35\%$  and  $Re_{\text{nf}} = 2000$

sections, NF temperature is found to intensify by augmenting the entering water temperature. The near wall regions experience higher temperature intensification

compared to the central region. In addition, Fig. 3 depicts that boosting the entering water temperature causes an intensification in the amount of NF temperature rise. This

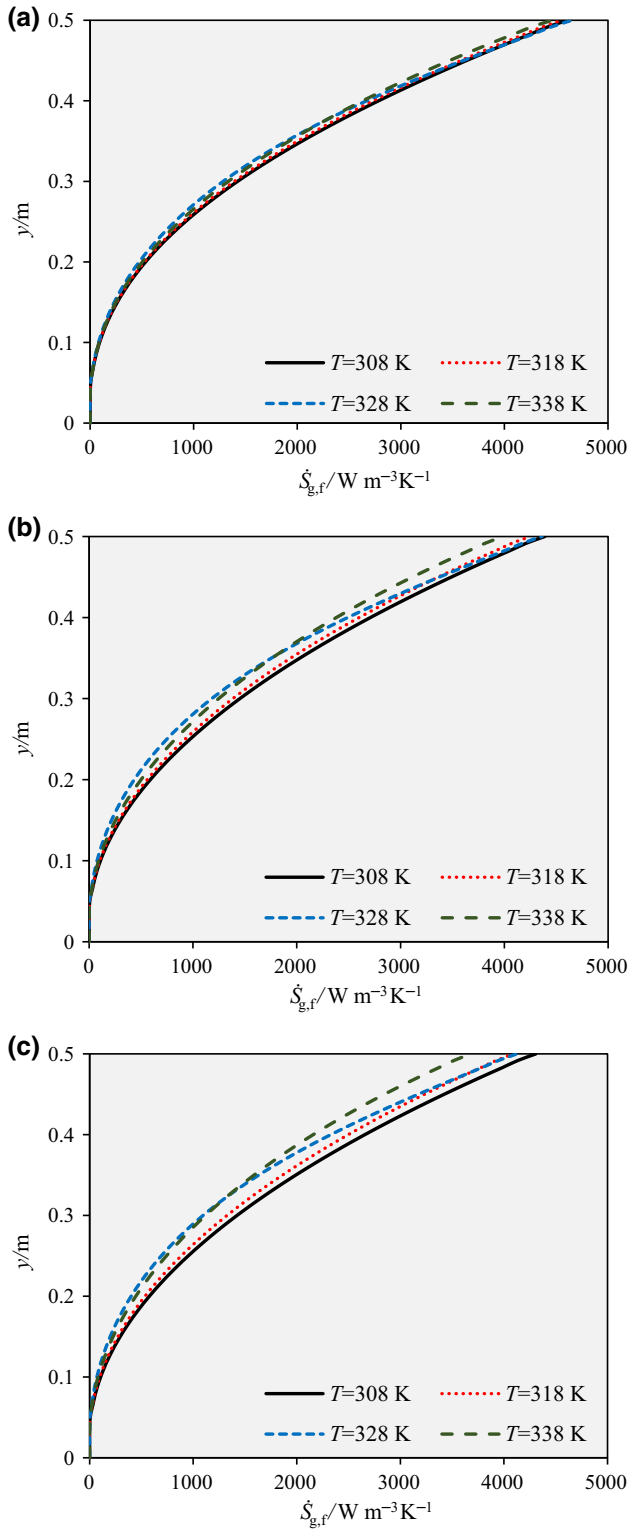


**Fig. 6** Variation of frictional irreversibility at cross section **a**  $x = 0.1\text{m}$ , **b**  $x = 0.5\text{m}$  and **c**  $x = 0.9\text{m}$  at various entering water temperatures for  $\varphi_{\text{FF}} = 0.9\%$ ,  $\varphi_{\text{CNT}} = 1.35\%$  and  $Re_{\text{nf}} = 2000$

can be attributed to the higher augmentation of thermal conductivity in these NFs. At a constant  $\varphi$ , the thermal conductivity coefficient of the NF only depends on its temperature and, as a result, both the thermal conductivity and temperature of NF have the same trend.

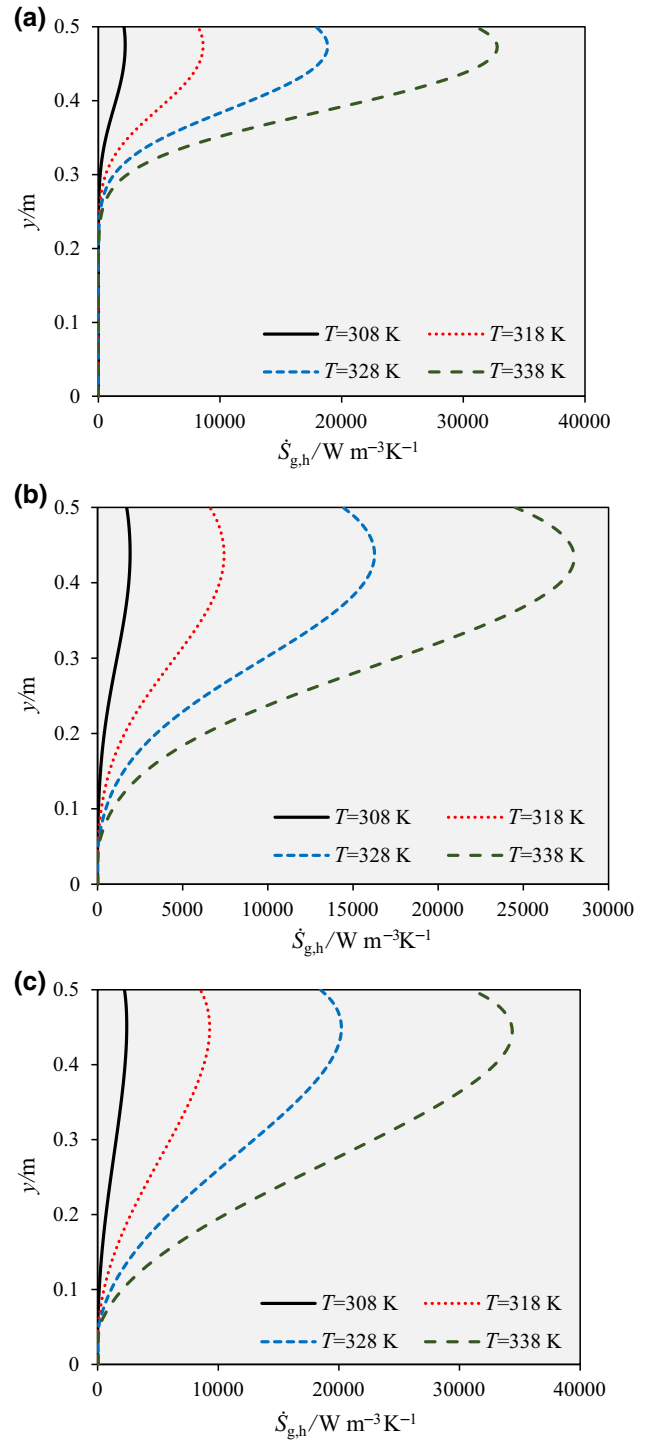


**Fig. 7** Variation of thermal irreversibility at cross section **a**  $x = 0.1\text{m}$ , **b**  $x = 0.5\text{m}$  and **c**  $x = 0.9\text{m}$  at various entering water temperatures for  $\varphi_{\text{FF}} = 0.9\%$ ,  $\varphi_{\text{CNT}} = 1.35\%$  and  $Re_{\text{nf}} = 2000$

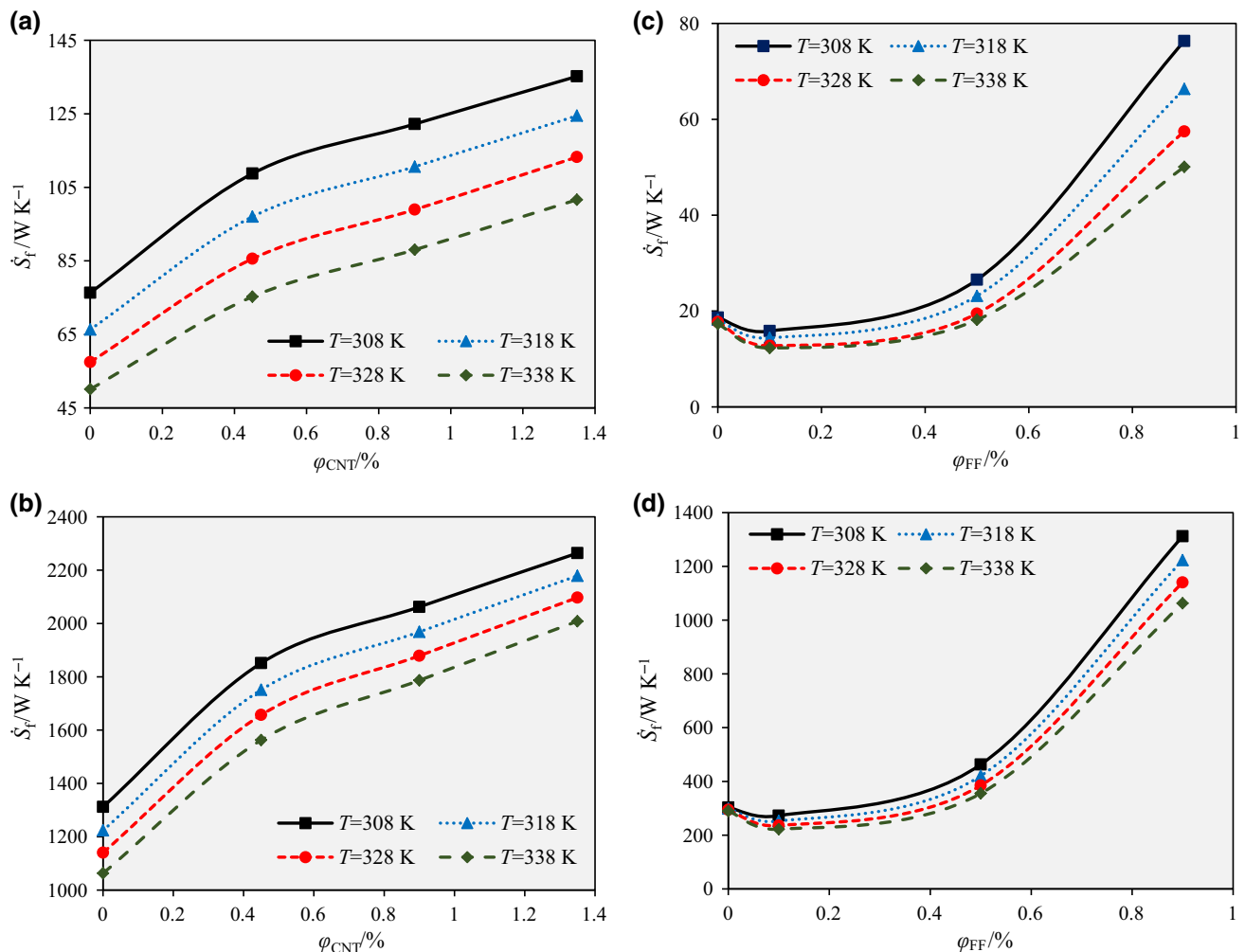
Figure 4 gives the NF viscosity in terms of entering water temperature along the cross sections  $x = 0.1, 0.5$  and  $0.9$  m. For all the examined cross sections, NF viscosity declines with boosting the entering water temperature. This is because of the intensification of NF temperature. Furthermore, the central region of tube experiences higher viscosity compared to the near wall region that is because of the higher velocity gradient in vicinity of the wall.

Figure 5 gives the NF velocity at cross sections  $x = 0.1, 0.5$  and  $0.9$  m versus entering water temperature. Boosting the entering temperature of water causes a decline in the velocity of NF near the tube center, while the opposite is true about the NF velocity in the vicinity of wall, which is because the reduction of viscosity near the wall.

The effects of entering water temperature rise on frictional irreversibility at cross sections  $x = 0.1, 0.5$  and  $0.9$  m are illustrated in Fig. 6. The pattern of variations of frictional irreversibility is the same for all the considered cross sections, so that:

- By intensifying the entering water temperature within the range of 308–318 K, the frictional irreversibility is decreased.
- By raising the entering water temperature within the range of 318–328 K, the frictional irreversibility is decreased except in the near-wall regions.
- By intensifying the entering water temperature within the range of 328–338 K, the frictional irreversibility is increased except in the near-wall regions.

According to Eq. (6), the frictional irreversibility is a function of NF viscosity, temperature and velocity gradient. As it was mentioned above, a rise in the temperature of entering water causes an intensification in the NF temperature and a decline in the NF viscosity and thus the reduction of frictional irreversibility. The reduction of NF viscosity near the tube wall leads to the intensification of NF velocity in this region and, ultimately, the decline of NF velocity near the tube center (due to the law of



**Fig. 8** Global frictional irreversibility versus nanoadditive volume fraction at various entering water temperatures for **a**  $Re_{nf} = 500$  and  $\phi_{FF} = 0.9\%$ , **b**  $Re_{nf} = 2000$  and  $\phi_{FF} = 0.9\%$ , **c**  $Re_{nf} = 500$  and  $\phi_{CNT} = 1.35\%$  and **d**  $Re_{nf} = 2000$  and  $\phi_{CNT} = 1.35\%$

conservation of mass). This results in the increase of velocity gradient and, thus, the increase of frictional irreversibility in the vicinity of wall. Therefore, the observed increase in the frictional irreversibility with the rise of entering water temperature can be attributed to the interactions between the effects of viscosity reduction, NF temperature rise and the increase of velocity gradient.

Figure 7 displays the thermal irreversibility at cross sections  $x = 0.1, 0.5$  and  $0.9$  m in terms of entering water temperature. It is observed that the thermal irreversibility of NF intensifies with augmenting the entering water temperature; which is something undesirable. According to Eq. (7), the thermal irreversibility is a function of NF's thermal conductivity, average temperature and temperature gradient. The temperature and the thermal conductivity of NF go up with the rise of entering water temperature, thereby reducing and increasing the thermal irreversibility, respectively. Also, the increase in the thermal conductivity coefficient of NF near the tube wall results in the reduction

of temperature gradient and thus the reduction of thermal irreversibility. Therefore, Fig. 7 reveals that the effect of the increase of thermal conductivity coefficient overcomes the effects of temperature rise and temperature gradient reduction, and that the thermal irreversibility intensifies with augmenting the entering water temperature. Figure 7 also shows that by moving from the tube center toward the wall, the thermal irreversibility increases at first, reaches a maximum value and then starts to decrease. The temperature and the thermal conductivity coefficient of NF are greater near the tube wall than near the tube center; this causes the reduction and the increase of thermal irreversibility near the tube wall, respectively. The temperature gradient and thus the thermal irreversibility of NF are also greater near the tube wall than near the tube center. Therefore, in view of Fig. 7, it can be concluded that by moving from the tube center toward the tube wall, first, the effects of the increase of thermal conductivity coefficient and temperature gradient outweighs the effect of

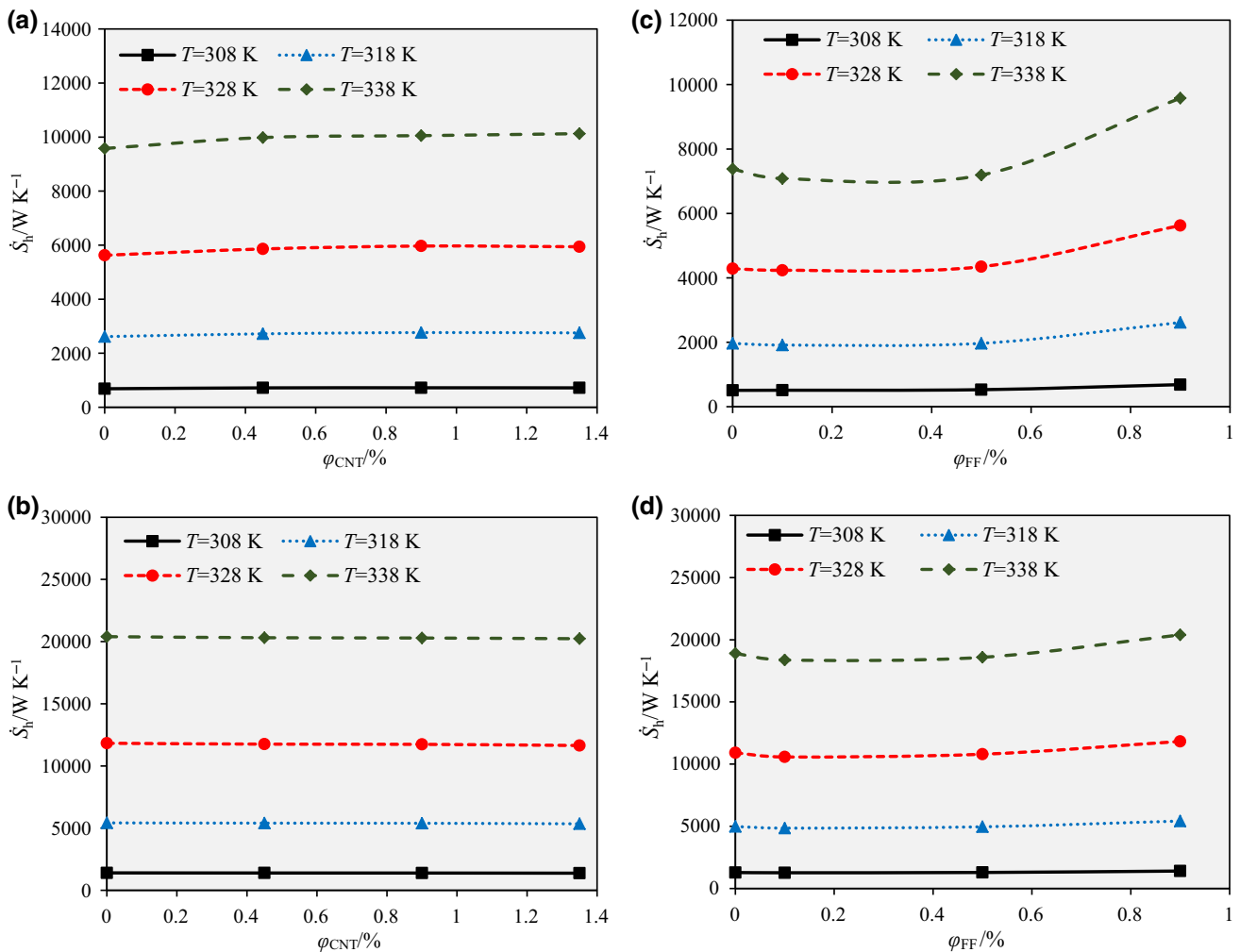


**Fig. 9** Global thermal irreversibility versus nanoadditive volume fraction at various entering water temperatures for **a**  $Re_{nf} = 500$  and  $\phi_{FF} = 0.9\%$ , **b**  $Re_{nf} = 2000$  and  $\phi_{FF} = 0.9\%$ , **c**  $Re_{nf} = 500$  and  $\phi_{CNT} = 1.35\%$  and **d**  $Re_{nf} = 2000$  and  $\phi_{CNT} = 1.35\%$

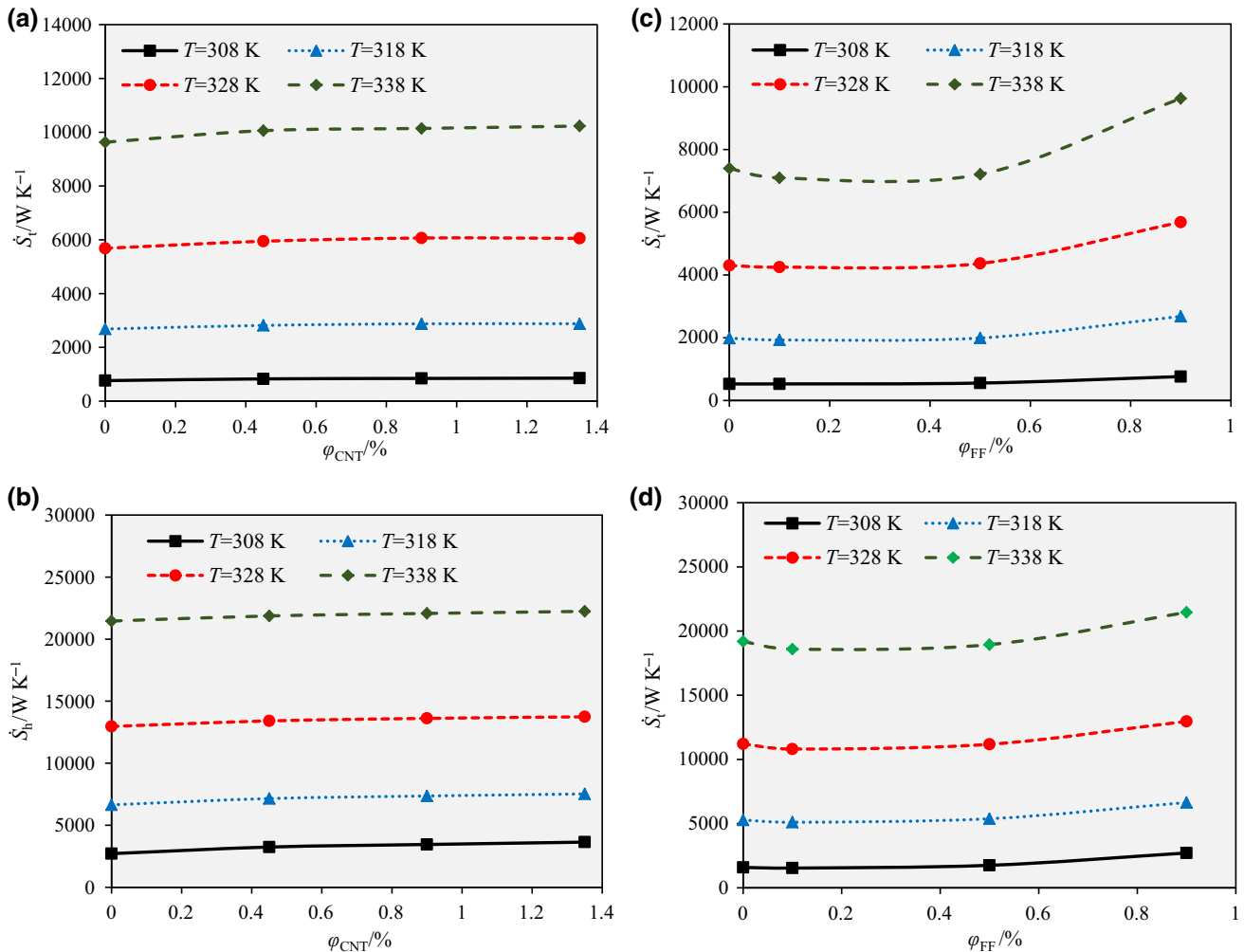
temperature rise, and the irreversibility increases; however, the opposite occurs near the tube wall.

Figure 8 shows the global frictional irreversibility versus entering water temperature in terms of  $\varphi_{\text{FF}}$ ,  $\varphi_{\text{CNT}}$  and  $Re_{\text{nf}}$ . According to the results, the frictional irreversibility of NF diminishes with intensifying entering water temperature. For instance, at  $\varphi_{\text{FF}} = 0.9\%$  and  $\varphi_{\text{CNT}} = 1.35\%$ , by intensifying the entering water temperature within the range of 308–338 K, the global frictional irreversibility at  $Re_{\text{nf}} = 500$  and  $Re_{\text{nf}} = 2000$  are reduced by 24.83% and 11.29%, respectively. The results also show that the increase of  $Re_{\text{nf}}$  and  $\varphi_{\text{CNT}}$  leads to the increase of global frictional irreversibility; while the increase of  $\varphi_{\text{FF}}$  first leads to the reduction and then the increase of global frictional irreversibility. Therefore, from the standpoint of irreversibility generation caused by friction, the best NF performance, at all the considered  $Re_{\text{nf}}$ , belongs to the pure water– $\text{Fe}_3\text{O}_4$  NF with  $\varphi_{\text{FF}} = 0.1\%$ .

Figure 9 displays the global thermal irreversibility versus entering water temperature in terms of  $\varphi_{\text{FF}}$ ,  $\varphi_{\text{CNT}}$  and  $Re_{\text{nf}}$ .

Obviously, the global thermal irreversibility increases with the intensification of entering water temperature. For instance, at  $\varphi_{\text{FF}} = 0.9\%$  and  $\varphi_{\text{CNT}} = 1.35\%$ , by augmenting the entering water temperature within the range of 308–338 K, the global thermal irreversibility at  $Re_{\text{nf}} = 500$  and  $Re_{\text{nf}} = 2000$  are increased by 1309.03% and 1370.5%, respectively. Moreover, the increase of  $Re_{\text{nf}}$  leads to the increase of thermal irreversibility; while the increase of  $\varphi_{\text{FF}}$  and  $\varphi_{\text{CNT}}$  first leads to the reduction and then the increase of global thermal irreversibility.

Figure 10 shows the global total irreversibility versus entering water temperature in terms of  $\varphi_{\text{FF}}$ ,  $\varphi_{\text{CNT}}$  and  $Re_{\text{nf}}$ . It is observed that the global total irreversibility increases with the rise of entering water temperature. Figure 10 also shows that the global total irreversibility increases with the increase of  $Re_{\text{nf}}$  and  $\varphi_{\text{CNT}}$ ; while the increase of  $\varphi_{\text{FF}}$  from zero to 0.1% causes a decline and the further increase of  $\varphi_{\text{FF}}$  leads to the increase of global total irreversibility. According to Fig. 10, the hybrid NF only has a desirable second law performance in the examined heat exchanger at



**Fig. 10** Global total irreversibility versus nanoadditive volume fraction at various entering water temperatures for **a**  $Re_{\text{nf}} = 500$  and  $\varphi_{\text{FF}} = 0.9\%$ , **b**  $Re_{\text{nf}} = 2000$  and  $\varphi_{\text{FF}} = 0.9\%$ , **c**  $Re_{\text{nf}} = 500$  and  $\varphi_{\text{CNT}} = 1.35\%$  and **d**  $Re_{\text{nf}} = 2000$  and  $\varphi_{\text{CNT}} = 1.35\%$

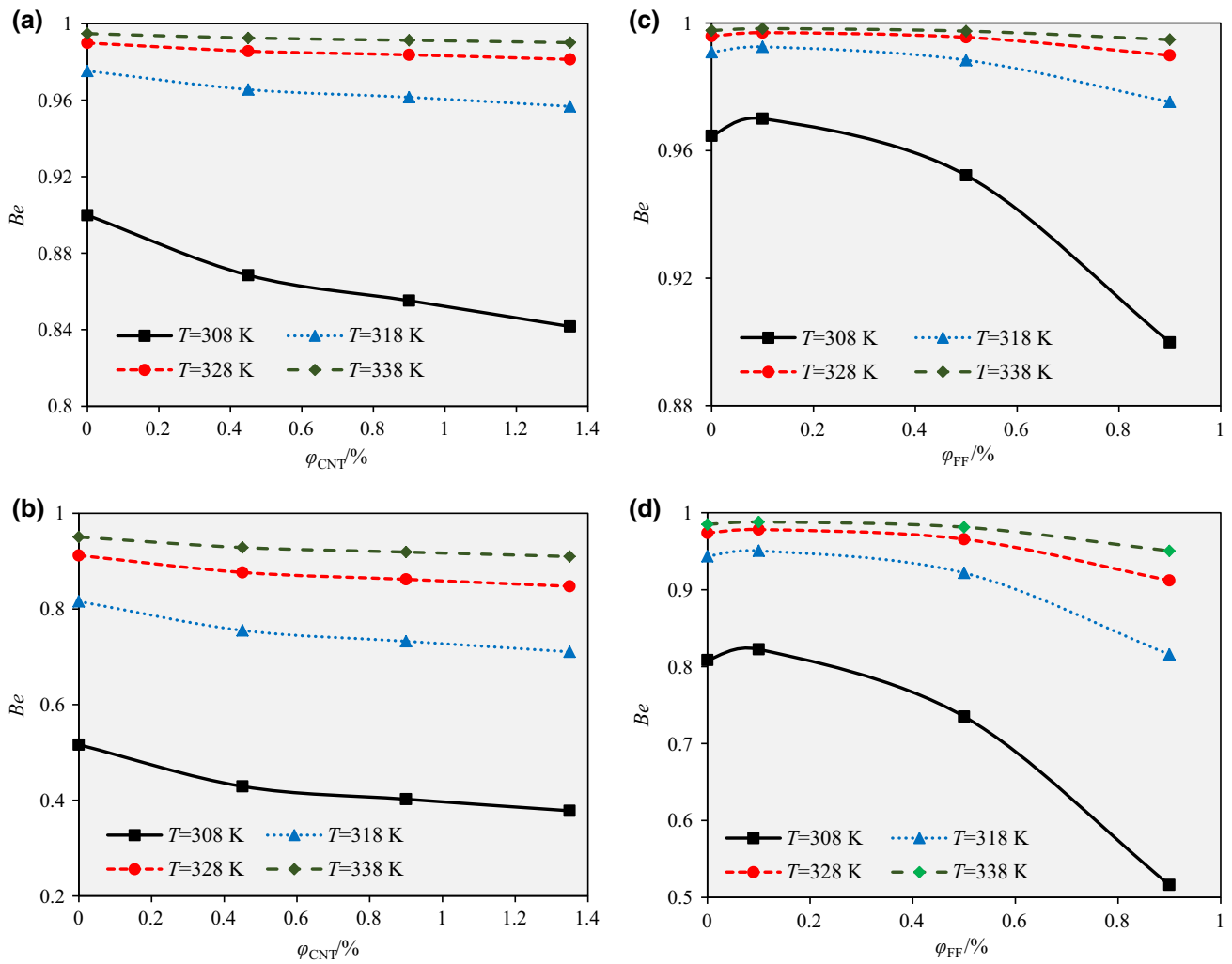


**Fig. 11** Global Bejan number versus nanoadditive volume fraction at various entering water temperatures for **a**  $Re_{nf} = 500$  and  $\phi_{FF} = 0.9\%$ , **b**  $Re_{nf} = 2000$  and  $\phi_{FF} = 0.9\%$ , **c**  $Re_{nf} = 500$  and  $\phi_{CNT} = 1.35\%$  and **d**  $Re_{nf} = 2000$  and  $\phi_{CNT} = 1.35\%$

$\phi_{FF} = 0.1\%$  and  $\phi_{CNT} = 0\%$ ; and the lower the  $Re_{nf}$ , the better the performance of hybrid NF.

Finally, Fig. 11 shows the impacts of entering water temperature on the Bejan number in terms of  $\phi_{FF}$ ,  $\phi_{CNT}$  and  $Re_{nf}$ . The Bejan number of NF intensifies by augmenting the entering water temperature; which means the greater share of heat transfer in the irreversibility generation, in comparison with flow friction. The results also reveal that the increase of  $Re_{nf}$ ,  $\phi_{CNT}$  and  $\phi_{FF}$  (except 0.1%) leads to the increase in the share of frictional irreversibility and, thus, the reduction of Bejan number.

## Conclusions

This numerical study is devoted to examine the impact of entering fluids temperature on the irreversibility characteristics of a minichannel HPHE. To this end, a counter-

flow HPHE was considered in which a cold water–CNT/ $Fe_3O_4$  hybrid NF flows in the tube side and hot water is pumped into the annulus. The entering NF temperature was considered as constant, and the entering water temperature was varied. The impacts of  $Re_{nf}$ ,  $\phi_{FF}$  and  $\phi_{CNT}$  on the obtained results were also assessed. By augmenting the entering water temperature, the temperature, thermal conductivity and local thermal irreversibility of NF increase, the NF viscosity reduces, and the NF velocity first increases and then reduces. In addition, it was found the boosting the entering water temperature causes an increase in the global thermal irreversibility, global total irreversibility and global Bejan number, while the frictional irreversibility reduces by intensifying the entering water temperature. Moreover, the findings revealed that the augmentation of  $Re_{nf}$  and  $\phi_{CNT}$  causes an increase in the global frictional and total irreversibilities and global Bejan number; while the augmentation of  $\phi_{FF}$  first leads to the

reduction and then the increase of these parameters. Furthermore, it was reported that augmentation of  $Re_{nf}$  results in an increase in the thermal irreversibility; while boosting the  $\varphi_{FF}$  and  $\varphi_{CNT}$  first leads to the reduction and then the increase of global thermal irreversibility.

**Acknowledgements** This work is partially supported by the National Key Research and Development Program of China (2016YFB0100903) and JITRI Suzhou Automotive Research Institute Project (CEC20190404).

## References

- Choi SUS. Enhancing thermal conductivity of fluids with nanoparticles. *ASME FED*. 1995;231:99–105.
- Al-Rashed AAAA, Shahsavari A, Rasooli O, Moghimi MA, Karimipour A, Tran MD. Numerical assessment into the hydrothermal and entropy generation characteristics of biological water–silver nano-fluid in a wavy walled microchannel heat sink. *Int Commun Heat Mass Transf*. 2019;104:118–26.
- Al-Rashed AAAA, Shahsavari A, Entezari S, Moghimi MA, Adio SA, Nguyen TK. Numerical investigation of non-Newtonian water–CMC/CuO nanofluid flow in an offset strip-fin microchannel heat sink: thermal performance and thermodynamic considerations. *Appl Therm Eng*. 2019;155:247–58.
- Alsarraf J, Moradikazerouni A, Shahsavari A, Afrand M, Salehipour H, Tran MD. Hydrothermal analysis of turbulent boehmite alumina nanofluid flow with different nanoparticle shapes in a minichannel heat exchanger using two-phase mixture model. *Phys A*. 2019;520:275–88.
- Nakhchi ME, Esfahani JA. Numerical investigation of turbulent Cu–water nanofluid in heat exchanger tube equipped with perforated conical rings. *Adv Powder Technol*. 2019;30:1338–47.
- Nakhchi ME, Esfahani JA. Cu–water nanofluid flow and heat transfer in a heat exchanger tube equipped with cross-cut twisted tape. *Powder Technol*. 2018;339:985–94.
- Nakhchi ME, Esfahani JA. Entropy generation of turbulent Cu–water nanofluid flow in a heat exchanger tube fitted with perforated conical rings. *J Therm Anal Calorim*. 2019. <https://doi.org/10.1007/s10973-019-08169-w>.
- Rashidi MM, Abelman S, Freidooni Mehr N. Entropy generation in steady MHD flow due to a rotating porous disk in a nanofluid. *Int J Heat Mass Transf*. 2013;62:515–25.
- Shahsavari A, Khanmohammadi S, Karimipour A, Goodarzi M. A novel comprehensive experimental study concerned synthesizes and prepare liquid paraffin-Fe<sub>3</sub>O<sub>4</sub> mixture to develop models for both thermal conductivity & viscosity: a new approach of GMDH type of neural network. *Int J Heat Mass Transf*. 2019;131:432–41.
- Shahsavari A, Khanmohammadi S, Toghraie D, Salehipour H. Experimental investigation and develop ANNs by introducing the suitable architectures and training algorithms supported by sensitivity analysis: measure thermal conductivity and viscosity for liquid paraffin based nanofluid containing Al<sub>2</sub>O<sub>3</sub> nanoparticles. *J Mol Liq*. 2019;276(2019):850–60.
- Sheikholeslami M, Rashidi MM, Ganji DD. Effect of non-uniform magnetic field on forced convection heat transfer of Fe<sub>3</sub>O<sub>4</sub>-water nanofluid. *Comput Methods Appl Mech Eng*. 2015;294:299–312.
- Garoosi F, Jahanshaloo L, Rashidi MM, Badakhsh A, Ali ME. Numerical simulation of natural convection of the nanofluid in heat exchangers using a Buongiorno model. *Appl Math Comput*. 2015;254:183–203.
- Freidoonimehr N, Rashidi MH, Mahmud S. Unsteady MHD free convective flow past a permeable stretching vertical surface in a nano-fluid. *Int J Therm Sci*. 2015;87:136–45.
- Shahsavari A, Salimpour MR, Saghafian M, Shafii MB. Experimental investigation on laminar forced convective heat transfer of ferrofluid loaded with carbon nanotubes under constant and alternating magnetic field. *Exp Therm Fluid Sci*. 2016;76:1–11.
- Rashed AM, Rashidi MM, Lorenzini G, Ahmed SE, Aly AM. Magnetic field and internal heat generation effects on the free convection in a rectangular cavity filled with a porous medium saturated with Cu–water nanofluid. *Int J Heat Mass Transf*. 2017;104:878–89.
- Shahsavari A, Moradi M, Bahiraei M. Heat transfer and entropy generation optimization for flow of a non-Newtonian hybrid nanofluid containing coated CNT/Fe<sub>3</sub>O<sub>4</sub> nanoparticles in a concentric annulus. *J Taiwan Inst Chem Eng*. 2018;84:28–40.
- Shahsavari A, Bahiraei M, Ansarian R. Effect of line dipole magnetic field on entropy generation of Mn–Zn ferrite ferrofluid flowing through a minichannel using two-phase mixture model. *Powder Technol*. 2018;340:370–9.
- Monfared M, Shahsavari A, Bahrebar MR. Second law analysis of turbulent convection flow of boehmite alumina nanofluid inside a double-pipe heat exchanger considering various shapes for nanoparticle. *J Therm Anal Calorim*. 2019;135:1521–32.
- Shahsavari A, Rahimi Z, Salehipour H. Nanoparticle shape effects on thermal-hydraulic performance of boehmite alumina nanofluid in a horizontal double-pipe minichannel heat exchanger. *Heat Mass Transf*. 2019;55:1741–51.
- Huminić G, Huminić A. Hybrid nanofluids for heat transfer applications—a state-of-the-art review. *Int J Heat Mass Transf*. 2018;125:82–103.
- Shahsavari A, Salimpour MR, Saghafian M, Shafii MB. An experimental study on the effect of ultrasonication on thermal conductivity of ferrofluid loaded with carbon nanotubes. *Thermochim Acta*. 2015;617:102–10.
- Shahsavari A, Saghafian M, Salimpour MR, Shafii MB. Effect of temperature and concentration on thermal conductivity and viscosity of ferrofluid loaded with carbon nanotubes. *Heat Mass Transf*. 2016;52:2293–301.
- Shahsavari A, Salimpour MR, Saghafian M, Shafii MB. Effect of magnetic field on thermal conductivity and viscosity of a magnetic nanofluid loaded with carbon nanotubes. *J Mech Sci Technol*. 2016;30:809–15.
- Liu WI, Alsarraf J, Shahsavari A, Rostamzadeh M, Afrand M, Nguyen TK. Impact of oscillating magnetic field on the thermal conductivity of water–Fe<sub>3</sub>O<sub>4</sub> and water–Fe<sub>3</sub>O<sub>4</sub>/CNT ferro-fluids: experimental study. *J Magn Magn Mater*. 2019;484:258–65.
- Karimi A, Al-Rashed AAAA, Afrand M, Mahian O, Wongwises S, Shahsavari A. The effects of tape insert material on the flow and heat transfer in a nanofluid-based double tube heat exchanger: two-phase mixture model. *Int J Mech Sci*. 2019;156:397–409.
- Shahsavari A, Godini A, Talebizadeh Sardari P, Toghraie D, Salehipour H. Impact of variable fluid properties on forced convection of Fe<sub>3</sub>O<sub>4</sub>/CNT/water hybrid nanofluid in a double-pipe mini-channel heat exchange. *J Therm Anal Calorim*. 2019;137:1031–43.
- Ma Y, Mohebbi R, Rashidi MM, Yang Z. MHD convective heat transfer of Ag–MgO/water hybrid nanofluid in a channel with active heaters and coolers. *Int J Heat Mass Transf*. 2019;137:714–26.
- Safaei MR, Hajizadeh A, Afrand M, Qi C, Yarmand H, Zulkifli NWBM. Evaluating the effect of temperature and concentration on the thermal conductivity of ZnO–TiO<sub>2</sub>/EG hybrid nanofluid using artificial neural network and curve fitting on experimental data. *Phys A*. 2019;519:209–16.

29. Nadooshan AA, Eshgarf H, Afrand M. Measuring the viscosity of  $\text{Fe}_3\text{O}_4$ -MWCNTs/EG hybrid nanofluid for evaluation of thermal efficiency: newtonian and non-Newtonian behavior. *Mol Liq.* 2018;253:169–77.
30. Esfahani NN, Toghraie D, Afrand M. A new correlation for predicting the thermal conductivity of ZnO–Ag (50%–50%)/water hybrid nanofluid: an experimental study. *Powder Technol.* 2018;323:367–73.
31. Goodarzi M, Kherbeet AS, Afrand M, Sadeghinezhad E, Mehrli M, Zahedi P, Wongwises S, Daheri M. Investigation of heat transfer performance and friction factor of a counter-flow double-pipe heat exchanger using nitrogen-doped, graphene-based nanofluids. *Int Commun Heat Mass Transf.* 2016;76:16–23.
32. Shahsavari A, Rahimi Z, Bahiraei M. Optimization of irreversibility and thermal characteristics of a mini heat exchanger operated with a new hybrid nanofluid containing carbon nanotubes decorated with magnetic nanoparticles. *Energy Convers Manag.* 2017;150:37–47.
33. Karimi A, Afrand M. Numerical study on thermal performance of an air-cooled heat exchanger: effects of hybrid nanofluid, pipe arrangement and cross section. *Energy Convers Manag.* 2017;164:615–28.
34. Diglio G, Roselli C, Sasso M, Channabasappa UJ. Borehole heat exchanger with nanofluids as heat carrier. *Geothermics.* 2018;72:112–23.
35. Rahimi A, Surendar A, Kasaeipoor A, Hooshmand P, Malekshahi EH. Lattice Boltzmann simulation of nanofluid flow and heat transfer in a hollow multi-pipe heat exchanger considering nanoparticles' shapes. *Powder Technol.* 2018;339:974–84.
36. Bahiraei M, Berahmand M, Shahsavari A. Irreversibility analysis for flow of a non-Newtonian hybrid nanofluid containing coated CNT/ $\text{Fe}_3\text{O}_4$  nanoparticles in a minichannel heat exchanger. *Appl Therm Eng.* 2017;125:1083–93.
37. Guzman JEV, Hernandez-Arrieta I, Vicente W, Salinas-Vazquez M, Martinez-Espinosa E. Non-local entropy evolution in heat exchangers with elliptical and circular tube geometries, international. *J Therm Sci.* 2018;134:601–11.
38. Dormohammadi R, Farzaneh-Gord M, Ebrahimi-Moghadam A, Ahmadi MH. Heat transfer and entropy generation of the nanofluid flow inside sinusoidal wavy channels. *J Mol Liq.* 2018;269:229–40.
39. Ebrahimi-Moghadam A, Jabari Moghadam A. Optimal design of geometrical parameters and flow characteristics for  $\text{Al}_2\text{O}_3$ /water nanofluid inside corrugated heat exchangers by using entropy generation minimization and genetic algorithm methods. *Appl Therm Eng.* 2019;149:889–98.
40. Al-Rashed AAAA, Ranjbarzadeh R, Aghakhani S, Soltanimehr M, Afrand M, Khang Nguyen T. Entropy generation of boehmite alumina nanofluid flow through a minichannel heat exchanger considering nanoparticle shape effect. *Phys A Stat Mech Appl.* 2019;521:724–36.
41. Shahsavari A, Bahiraei M. Experimental investigation and modeling of thermal conductivity and viscosity for non-Newtonian hybrid nanofluid containing coated CNT/ $\text{Fe}_3\text{O}_4$  nanoparticles. *Powder Technol.* 2017;318:441–50.
42. Shahsavari A, Talebizadeh P, Toghraie D. Free convection heat transfer and entropy generation analysis of water– $\text{Fe}_3\text{O}_4$ /CNT hybrid nanofluid in a concentric annulus. *Int J Numer Methods Heat Fluid Flow.* 2019;29:915–34.
43. Duangthongsuk W, Wongwises S. An experimental study on the heat transfer performance and pressure drop of  $\text{TiO}_2$ –water nanofluids flowing under a turbulent flow regime. *Int J Heat Mass Transf.* 2010;53:334–44.

**Publisher's Note** Springer Nature remains neutral with regard to jurisdictional claims in published maps and institutional affiliations.